Available online at www.sciencedirect.com
ScienceDirect
Ceramics International 38 (2012) 251–258
CERAMICS INTERNATIONAL
www.elsevier.com/locate/ceramint

Influence of barium oxide on the crystallization, microstructure and mechanical properties of potassium fluorophlogopite glass–ceramics

P.K. Maiti [a,*], Amit Mallik [a], A. Basumajumdar [a], P. Guha [b]

[a] Ceramic Engineering Division, Dept. of Chemical Technology, University of Calcutta, 92, A. P. C. Road, Kolkata 700009, India
[b] Govt. College of Engineering and Ceramic Technology, 73, A. C. Banerjee Lane, Kolkata 700010, India

Received 22 April 2011; received in revised form 26 June 2011; accepted 28 June 2011
Available online 12th July 2011

Abstract

The influence of barium oxide, heat treatment time and temperature on the crystallization, microstructure and mechanical behavior of the system $Ba_x{\cdot}K_{1-2x}{\cdot}Mg_3{\cdot}Al{\cdot}Si_3O_{10}{\cdot}F_2$ (where $x = 0.0$, 0.3 and 0.5) was investigated in order to develop novel, high strength and machinable glass–ceramics. Three glasses were prepared and characterized by differential thermal analysis (DTA), X-ray diffraction (XRD), scanning electron microscope (SEM) techniques and some mechanical testing methods.

The crystallization kinetics of glass–ceramics was also studied. Activation energy and Avrami exponent calculated for the crystallization peak temperature (T_p) of three different glass batches. The Vickers hardness decreased slightly on formation of the potassium fluorophlogopite and barium fluorophlogopite phases, but decreased significantly on formation of an interconnected 'house of cards' microstructure.

Keywords: B. Microstructure-final; C. Hardness; D. Glass; D. Glass–ceramics

1. Introduction

The controlled crystallization of glass produced mica glass–ceramics. Glasses based on the system $K_2O{\cdot}MgO{\cdot}Al_2O_3{\cdot}SiO_2{\cdot}MgF_2$ crystallize to trisilicic alkaline phlogopite mica ($K{\cdot}Mg_3{\cdot}Al{\cdot}Si_3{\cdot}O_{10}{\cdot}F_2$) glass–ceramics. These glass–ceramics have an important feature, which made them machinable to a precise tolerance with traditional metal working tools [1]. The microstructure of this phlogopite mica crystals precipitate in a 'house of cards' microstructure, embedded in a glass matrix, facilitates microfracture along the weak mica–glass interface and also through mica basal planes, which resists macroscopic failure during machining.

Beall [2] undertook the first studies of the alkali earth fluormica glass–ceramics. Later on Hoda and Beall [3] investigated different compositions containing barium, calcium, and strontium glasses close in composition to the respective fluorophlogopite stoichiometry. Most of the compositions were susceptible to crystallization during casting.

Uno et al. [4] investigated glass–ceramics containing barium-mica in the system $Ba_{0.5}{\cdot}Mg_3{\cdot}(Si_3{\cdot}AlO_{10}){\cdot}F_2$–$Mg_2{\cdot}Al_4{\cdot}Si_5{\cdot}O_{18}$–$Ca_3(PO_4)_2$. They found improved fracture toughness and bending strength values. Addition of tricalcium phosphate $Ca_3(PO_4)_2$ was claimed to improve the stability of the glasses prior to crystallization. But no specific compositional details were given. However it was stated that the compositions were close to the $Ba_{0.5}{\cdot}Mg_3{\cdot}(Al{\cdot}Si_3){\cdot}O_{10}{\cdot}F_2$ stochiometry.

Henry and Hill [5,6] have shown that reducing the alumina content reduces the glass transition temperature, first peak crystallization temperature and promotes bulk crystal nucleation. The glasses with high alumina contents gave rise to feathery microstructures that did not coarsen readily to give blocky crystals of a high aspect ratio and therefore could not produce the classic 'house of cards' microstructure. Hardness and machinability were found to be highly dependent on the formation of an interconnected 'house of cards' microstructure.

In the previous work [7], we have studied the kinetics as well as the crystal growth with respect to fluorine content in the barium fluorophlogopite glass–ceramics based on the system $BaO{\cdot}4MgO{\cdot}Al_2O_3{\cdot}6SiO_2{\cdot}2MgF_2$, where it was indicated that the crystallization of the glass was largely homogenous and fluorine promotes initial crystallization.

* Corresponding author. Tel.: +91 9432889369; fax: +91 3323519755.
E-mail address: prabir.maiti@gmail.com (P.K. Maiti).

0272-8842/$36.00
doi:10.1016/j.ceramint.2011.06.060

Greene et al. [8] investigated molar volume (MV), fractional glass compactness (C), microhardness (μH_v), glass transition temperature (T_{gmid}) and co-efficient thermal expansion (α) in the $(1-Z)BaO{:}ZK_2O{:}(6-X)MgO{:}XMgF_2{:}(3-Q)Al_2O_3{:}QB_2O_3{:}8SiO_2$ system (where $Z = 0, 0.25, 0.5, 0.75$ and $1.0, X = 2, 2.5$ and 3.0 and $Q = 0$, 0.5 and 1). Substitution of barium by potassium results in increases in molar volume and co-efficients of thermal expansion and decreases in fractional glass compactness, micro hardness and glass transition temperature values.

But very little or no work has been done on the system containing both potassium and barium to study the crystallization, microstructure and mechanical properties. The aim of this present study was to systematically investigate the effects of substituting barium for potassium in the above-mentioned compositions on their crystallization, microstructure and mechanical properties.

2. Experimental

2.1. Glass synthesis

The glass-forming compositions studied are represented by the following generic formula:

$$Ba_x{\cdot}K_{1-2x}{\cdot}Mg_3{\cdot}(Al\cdot Si_3)\cdot O_{10}{\cdot}F_2$$

where x varies among 0.0, 0.3 and 0.5 as shown in Table 1. For this study, the glasses were synthesized using the analytical grade reagents, barium carbonate ($BaCO_3$), potassium carbonate (K_2CO_3), silica (SiO_2), magnesium carbonate ($MgCO_3$), alumina (Al_2O_3), magnesium fluoride (MgF_2) and boric acid (H_3BO_3) powders mostly from E. Merck, mixed thoroughly in an attrition mill. In all the batches, B_2O_3 as H_3BO_3, was added purposefully to reduce the viscosity and thereof to increase the rate of diffusion of different ionic species in glass, which may result in the natural tendency towards directional growth of crystals [9]. The different batches were melted in a platinum crucible in an electrically heated furnace, melt was kept at the maximum melting temperature of 1500 °C for 2 h with occasional stirring with a platinum rod to homogenise the melt. The melts were poured in to a hot iron mould to make glass block of about 60 mm × 25 mm × 10 mm dimension. After releasing from the mould, the glass blocks were immediately transferred to an annealing furnace operating at a temperature 50 °C below the midpoint of the glass transition region and held for 1 h at the temperature followed by natural cooling to room temperature.

After annealing, the blocks were cut into pieces to about 2 mm thickness. These plates were fired for nucleation at 670 °C for Ba00, 700 °C for Ba03 and 720 °C for Ba05 batches respectively for 2 h. Subsequently heated to the corresponding crystallization temperature at a rate of 2 °C/min and the samples were kept at the crystallization temperature for 5 h and followed by natural cooling to room temperature.

Table 1
Chemical composition of the glass batch (in g).

Sample label	$BaCO_3$	K_2CO_3	MgO	Al_2O_3	SiO_2	MgF_2	H_3BO_3
Ba00	0.0	16.76	19.69	12.35	42.81	15.10	2.01
Ba03	13.64	6.42	18.93	11.86	41.06	14.47	2.01
Ba05	22.20	0.0	18.51	11.57	40.18	13.71	2.01

2.2. Characterization techniques

2.2.1. Differential thermal analysis (DTA)

Differential thermal analysis (DTA) was done using Shimadzu DT40 thermal analyzer against α-alumina powder as reference material. The three different resulting glasses were crushed and finally ground to ∼75 μm suitable for DTA. Non-isothermal experiments were performed by heating about 17 mg sample, at a heating rate of 5, 10, 15 and 20 °C/min in the temperature range from ambient to 1000 °C. Differential thermal analysis (DTA) was applied to calculate the value of activation energy by Kissinger equation and to calculate the Avrami exponent by Augis–Bennet equation.

2.2.2. X-ray powder diffraction (XRD)

Five heat treatment temperatures were investigated by X-ray powder diffraction on powder samples. All samples were heat treated using a heating rate of 10 °C/min to the nucleation temperature (above mentioned), soaked for 2 h at this temperature, heated again at 2 °C/min to the corresponding crystallization temperature and was kept at the temperature for 5 h followed by natural cooling to room temperature. XRD experiments were performed using X-ray powder diffractometer (PW 1830, Panalytical) using Ni filter Cukα_1, X-radiation with scanning speed of 2° (2θ) per minute. The diffraction pattern was recorded within Bragg angle range $10^\circ < 2\theta < 70$. The phases identified by JCPDS numbers (ICDD–PDF2 data base).

2.2.3. Scanning electron microscopy (SEM)

Samples from all the crystallization temperature (heating schedule as mentioned earlier) were studied to investigate the microstructural development with back scattered electron imaging (BEI) mode in a scanning electron microscope, Hitachi, S3400N, Japan. Before analysis, surface of all the samples was polished with diamond paste. The samples etched chemically by HF solution for 15 s.

2.2.4. Microindentation hardness and machinability measurement

Micro hardness analyses were carried out on polished glass samples embedded in epoxy resin using LEITZ micro hardness indenter. A load (P) of up to 500 g was used in conjunction with Vickers diamond indenter (face angle 136°) for 15 s. Hardness values were calculated using the following relation [10,11]

$$H_v = 1.8544 \times \frac{P}{D^2} \quad (1)$$

where H_v is the Vickers hardness number in kg/mm^2, P is the normal load in kg, and D is the length of the diagonal of the

indentation in mm. To convert the H_v into GPa the following relation was used

$$H_v\ (\text{GPa}) = \frac{9.81}{1000} \times H_v \tag{2}$$

The machinability parameter (m) can also be used for the effects of various heat treatments as a function of temperature and H_v. Machinability can be predicted by the micro hardness data. The following equation indicates the relationship between hardness (H_v) and machinability (m).

$$m = 0.643 - 0.122H_v \tag{3}$$

The fracture toughness (K_{IC}) is calculated using the following formula:

$$K_{IC} = \frac{0.025P}{c^{1.5}} \tag{4}$$

where c is the average crack length in mm.

3. Results and discussion

3.1. Kinetics of crystallization

DTA curves for three different glass samples at a heating rate of 5, 10, 15 and 20 °C/min are shown in Fig. 1a–c respectively. Only one exothermic peak was observed in both Ba00 and Ba05 batches. The exothermic peak corresponds to potassium fluorophlogopite and barium fluorophlogopite in Ba00 and Ba05 respectively. But two exothermic peaks are visible in Ba03. The first one is for potassium fluorophlogopite and second one is for barium fluorophlogopite [12]. The precipitation of crystal phases depends upon the ionic mobility of cations. The crystallization peak for K-fluorophlogopite appeared first in the DTA thermogram of the batch Ba03 because the ionic mobility of K^+ is higher compared to that of Ba^{2+}, due to smaller cationic size of the former. In the DTA thermograms, heating rate at 10 °C/min, the 1st exothermic peak of Ba03, which is supposed to be for K-fluorophlogopite, is shifted towards higher temperature approximately by 55 °C compared to the exothermic peak of Ba00 (Fig. 1a and b; Table 2). But the 2nd exothermic peak of Ba03, which is identified as Ba-fluorophlogopite, is shifted towards higher temperature approximately by 4 °C compared to that of Ba05 (Fig. 1b and c; Table 2). The first cause of shifting of peaks might be due to the higher viscosity of the glass imposed by the presence of barium. The 2nd cause, though insignificant, might be due to the hindrance encountered by the counter ions, i.e. Ba^{2+} and K^+ during the formation of their corresponding crystal phases. In case of 2nd peak, the shifting is only by 4 °C compared to that of 1st peak, which might be due to the significant lowering of viscosity at higher temperature.

The activation energy for the crystal growth of the samples Ba00 and Ba05 was estimated to be 209.1 kJ mol^{-1} and 304.9 kJ mol^{-1}, which is lower than the value obtained by Bagdassarov [13] (245 kJ mol^{-1}) and Henry and Hill [12] (307 kJ mol^{-1}). The discrepancy in these values might be arising form the different chemical compositions [14].

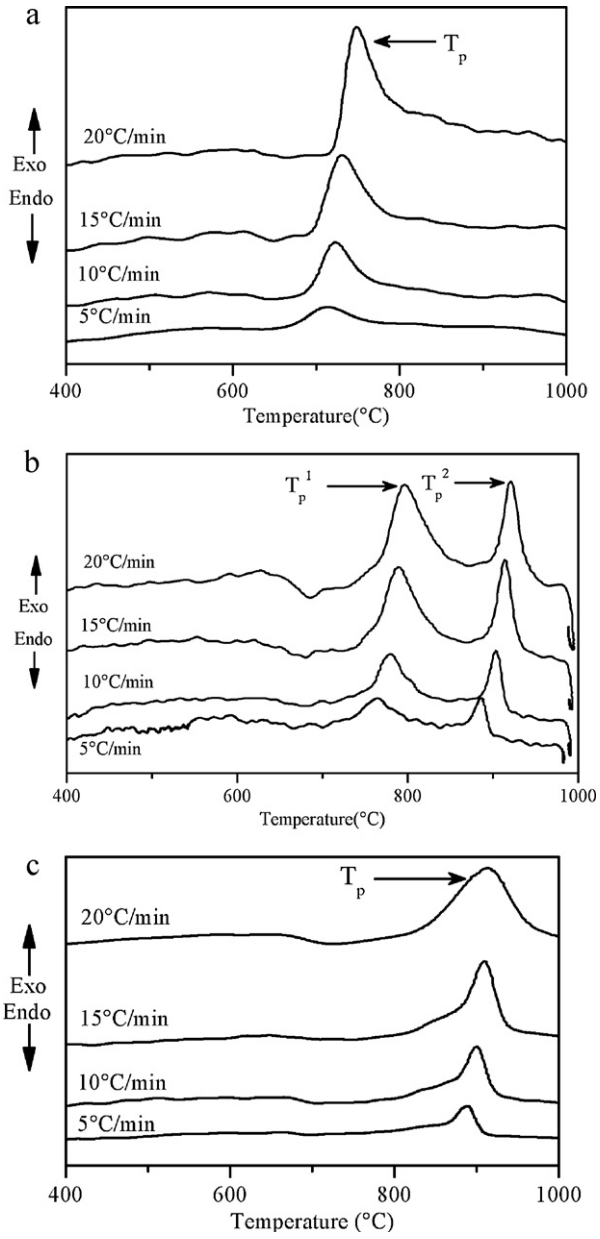

Fig. 1. Differential thermal analysis plots of glass samples of varying heating rate for (a) Ba00, (b) Ba03 and (c) Ba05.

From these curves, it is visible that the glass transition temperature (T_g) and crystallization peak temperature (T_p) shifted towards right with increasing heating rate.

The activation energy (E) of crystallization was calculated using the following modified form of Kissinger equation established by Matusita and Saka [15].

$$\ln\frac{T_p^2}{\beta} = \frac{E}{RT_p} + C \tag{5}$$

where β is the heating rate, R is the universal gas constant. The Avrami exponent (n) was calculated using the value activation energy (E) by the Augis–Bennett equation [16].

$$n = \frac{2.5}{\Delta T} \times \frac{RT_p^2}{E} \tag{6}$$

Table 2
Values of activation energy (Kissinger [E_k]) and Avrami exponent.

Sample label	Heating rate (β) (°C/min)	1st crystallization peak temperature $\left(T_p^1\right)$ (K)				2nd crystallization peak temperature $\left(T_p^2\right)$ (K)			
		T_p^1 (K)	Activation energy (kJ mol^{-1})	Avrami exponent (n)	$\langle n \rangle$	T_p^2 (K)	Activation energy (kJ mol^{-1})	Avrami exponent (n)	$\langle n \rangle$
Ba00	5	713 ± 2	209.1 ± 3	2.83	2.93 ≈ 3.00	0	0.0	0.0	0.0
	10	723 ± 2		2.93		0		0.0	
	15	732 ± 2		3.03		0		0.0	
	20	740 ± 2		3.13		0		0.0	
Ba03	5	763 ± 2	197.2 ± 3	2.63	2.9 ≈ 3.00	886 ± 2	250.4 ± 3	3.77	3.94 ≈ 4.00
	10	779 ± 2		2.83		903 ± 2		3.87	
	15	789 ± 2		2.93		913 ± 2		3.97	
	20	796 ± 2		3.00		921 ± 2		4.17	
Ba05	5	890 ± 2	304.9 ± 3	3.43	3.72 ≈ 4.00	0	0.0	0.0	0.0
	10	901 ± 2		3.63		0		0.0	
	15	912 ± 2		3.83		0		0.0	
	20	918 ± 2		4.00		0		0.0	

where n is the Avrami exponent or crystallization index and ΔT is the full width of the exothermic peak at the half-maximum intensity. The crystallization index (n) depends upon the actual nucleation and growth mechanism. According to JMA theory, crystallization index (n) is also related to crystallization manner, $n \cong 2$ means that the surface crystallization dominates overall crystallization, $n \cong 3$ means that the two dimensional crystallization or volumetric crystallization, $n \cong 4$ means that the three dimensional crystallization for bulk materials [17–19].

The Avrami exponent and activation energy were calculated using the above equations and shown in Table 2. In Ba00 and Ba03, for the 1st crystallization peak temperature (T_p), Avrami exponent was 2.93 and 2.90 respectively, which are close to 3, therefore the fact indicates that bulk nucleation and two dimensional growth occurs for the glass–ceramics.

From 2nd crystallization peak temperature, Avrami exponent was found to be 3.94 and 3.72 for Ba03 and Ba05 respectively, which are close to 4, therefore the fact indicates that it is a case of bulk nucleation and three dimensional crystal growths for the material concerned.

3.2. Results of X-ray diffraction

In Ba00, at 800 °C, peaks of K-fluorophlogopite ($KMg_3AlSi_3O_{10}F_2$) (JCPDS reference-00-019-0117) appeared as a major phase. The amount of this phase increases with increasing heat treatment temperature as shown in Fig. 2a. At 900 °C, several peaks of K-fluorophlogopite at 19.5°, 23.2°, 32.6°, 35.8°, 36.7°, and 45.4° and one peak of enstatite (JCPDS reference-00-002-0546) at 63° appeared along with K-fluorophlogopite. At 1000 °C, peaks of K-fluorophlogopite at 17.7°, 26°, 27.4°, 30.8°, 31.6°, 41.9° and 55.2° and one peak of mullite (JCPDS reference-00-001-0613) at 16.6° appeared along with K-fluorophlogopite. At 1100 °C, there are no changes in the intensity of the peaks but one peak of K-fluorophlogopite appeared at 57.1°. From 1100 °C to 1150 °C, there are no changes in the intensity of the peaks but the sharpness of the peaks has been increased.

In Ba03, at 800 °C, peaks of K-fluorophlogopite appeared at 27° and 34° as a major component whereas, Ba-fluorophlogopite (JCPDS reference-00-019-0117) appeared as a minor component and one peak of barium aluminium silicate (JCPDS reference-00-026-0137) appeared at 11.4° as shown in Fig. 2b. At 900 °C, two peaks of alpha-hexacelsian appeared at 22.7° and 30.0° along with Ba-fluorophlogopite, K-fluorophlogopite and barium aluminium silicate. At 1000 °C, two fresh peaks of Ba-fluorophlogopite at 17.4° and 36.7°, one peak of K-fluorophlogopite at 25.8°, one peak of alpha-hexacelsian (JCPDS reference-01-088-1050) at 54° and two peaks of enstatite at 35.8° and 34.4° appeared along with Ba-fluorophlogopite and K-fluorophlogopite but a peak of barium aluminium silicate at 11.4° disappeared. From 1000 °C to 1100 °C, there are no changes in the intensity of the peaks but one peak of K-fluorophlogopite at 41.9° and a peak of enstatite at 63° appeared. From 1100 °C to 1150 °C, there are no changes in the intensity of the peaks but the sharpness of the peaks has been increased.

In Ba05, the formation of Ba-fluorophlogopite phase is dominant in all heat treatment temperatures, and the amount of this phase increased with increasing heat treatment temperature as shown in Fig. 2c. At 800 °C, peaks of enstatite appeared at 40.9° and barium aluminium silicate appeared at 11.4°, 22.4°, and 29.8° along with barium fluorophlogopite. From 800 °C to 1000 °C there is no change in the intensity of the peaks and no new phases appeared. At 1100 °C, one new peak of barium fluorophlogopite appeared at 26.9° along with remaining other peaks. But at 1100 °C and 1150 °C, the sharpness of the peaks of both barium aluminium silicate and enstatite has been increased.

The formation of K-fluorophlogopite and Ba-fluorophlogopite is major phases in Ba00 and Ba05 respectively. But both the phases viz. K-fluorophlogopite and Ba-fluorophlogopite appeared in Ba03 simultaneously. With increasing heat treatment temperature, the formation of K-fluorophlogopite increased but the formation of Ba-fluorophlogopite is decreased.

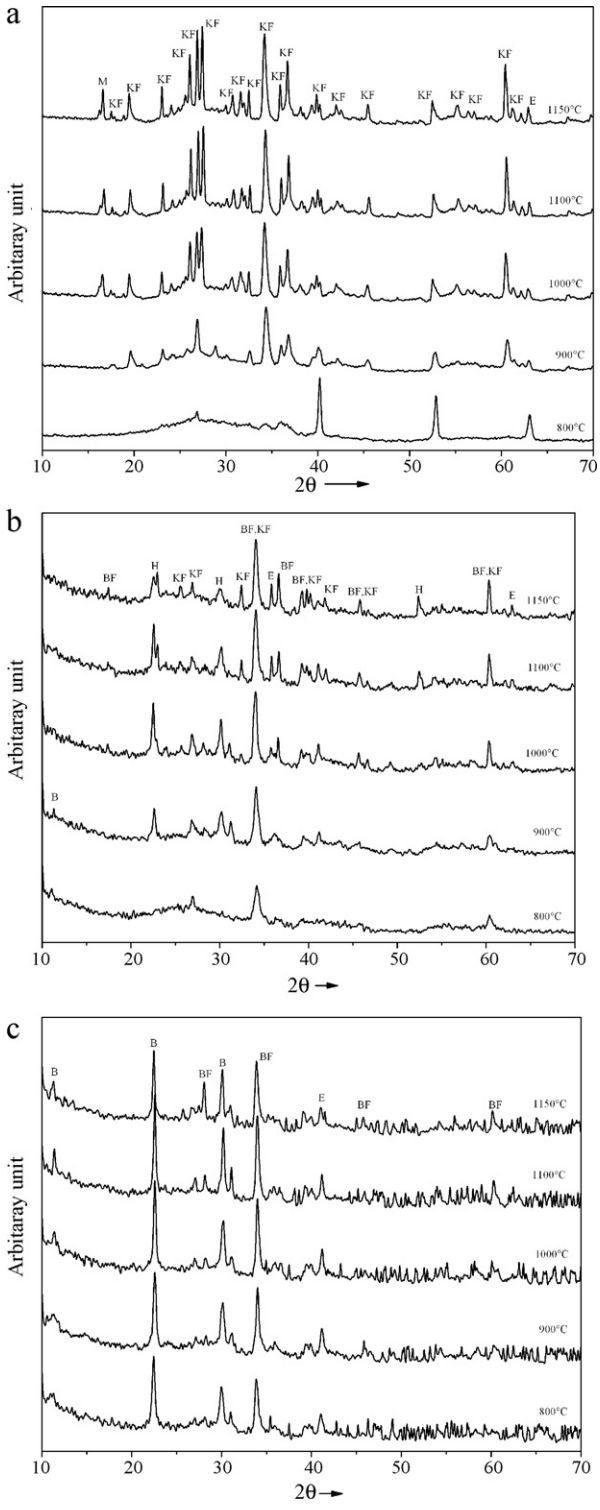

Fig. 2. XRD patterns for glass samples at different crystallization temperatures (a) Ba00, (b) Ba03 and (c) Ba05 [KF: potassium fluorophlogopite, BF: barium fluorophlogopite, M: mullite, E: enstatite B: barium aluminium silicate and H: alpha-hexacelsian].

3.3. Microstructure analysis

In Ba00, Ba03 and Ba05 samples heated at 800 °C for 5 h exhibit very fine submicron microstructures consists of some blocky crystal (Figs. 3a, 4a and 5a). Samples heated at 900 °C and 1000 °C for 5 h exhibited a large number of slightly bigger blocky crystals compared to that of at 800 °C (Figs. 3b, 4b and c and 5b and c). But the sample Ba00 formed large sized longer crystals at 1000 °C (Fig. 3c). These crystals are dense and appeared white in the back scattered electron micrographs with more or less low aspect ratio in highly siliceous residual glass with acicular morphology. Samples heated at 1150 °C for 5 h exhibited large sized crystals with high aspect ratio in highly siliceous residual glass with acicular morphology (Figs. 3d, 4d and 5d).

As the temperature increased, the crystal size increased along with the aspect ratio (length/diameter) of the crystals increased (Figs. 3a and b, 4a–c and 5a–c). It might be due to the dissolution of crystals with an aspect ratio of <1 and reprecipitation of constituents onto these crystals of higher aspect ratio. This energetically unfavorable configuration might therefore be the driving force towards attaining the long crystal observed after treatment for 5 h at 1000 °C and 1150 °C for Ba00, and 1150 °C for Ba03 and Ba05 (Figs. 3c and d, 4d and 5d), which is also discussed elsewhere [20].

According to the study, crystal growth or the growth index [21,22] of mica was 3 and 4, which indicates that the mica crystals grew along two and three dimensions respectively. Therefore most mica based glass–ceramics possessed ‘plate like’ and ‘house of cards’ microstructure [4,23,24]. The aspect ratios and size of mica crystals were considerably much dependent on the viscosity of melt. As the crystallization temperature increased, the viscosity of melt decreased. Then the diffusion of ions from glass matrix to crystal was easy to realize, the size of mica crystals increased.

3.4. Hardness and machinability measurement

Generally it is observed that at 800 °C, the Vickers hardness values reduces to a large extent on formation of the either potassium or barium, or both potassium and barium fluorophlogopite phases compared to that of original glasses. When the temperature is further increased, the Vickers hardness values gradually decreases up to 1100 °C. The hardness values increases slightly beyond this temperature up to 1150 °C (Fig. 6), but the increase is very low and sufficiently lower than that of the original glasses. The large reduction in hardness value correlates with the formation of the interconnected ‘‘house of cards’’ microstructure [6]. At any particular temperature, the hardness values increases with gradual increase in barium content.

In all the batches for different heat treatment temperatures, the machinability parameter (Fig. 6) was calculated from Vickers hardness (H_v) values. It is clear from the results that the higher the hardness values the lower the machinability parameter, whereas, at any particular temperature the machinability decreases with gradual increase in barium content. In all the batches for different heat treatment temperatures, the fracture toughness (Fig. 6) calculated from Vickers hardness (H_v) values. It is clear from the results that the higher the hardness values the higher the fracture toughness. At any particular temperature the fracture toughness increases with gradual increase in barium content. Invariably in all the batches,

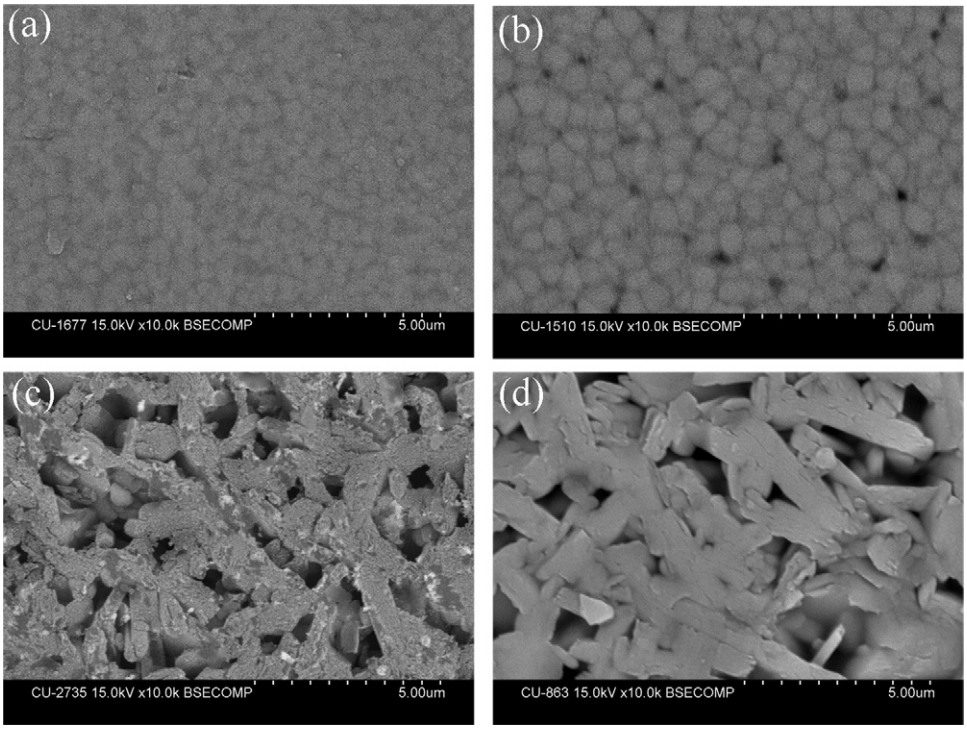

Fig. 3. SEM photograph of polished and etched surface of Ba00 nucleated at 670 °C for 2 h and crystallized at 800 °C (a), 900 °C (b), 1000 °C (c), and 1150 °C (d) for 5 h.

crystallized at 1150 °C, the sudden increase in hardness values might be due to the formation of other crystal phases like insatiate and barium aluminium silicate, etc.

The hardness decreases with increasing aspect ratio of the crystal and the crystallinity of mica, and the machinability also increases. The glass–ceramics showing negative values of m cannot be considered to be machinable, because they need a large threshold cutting force to initiate machining and are difficult to machining to intricate shapes. On the other hand, samples having positive m can be machined precisely by

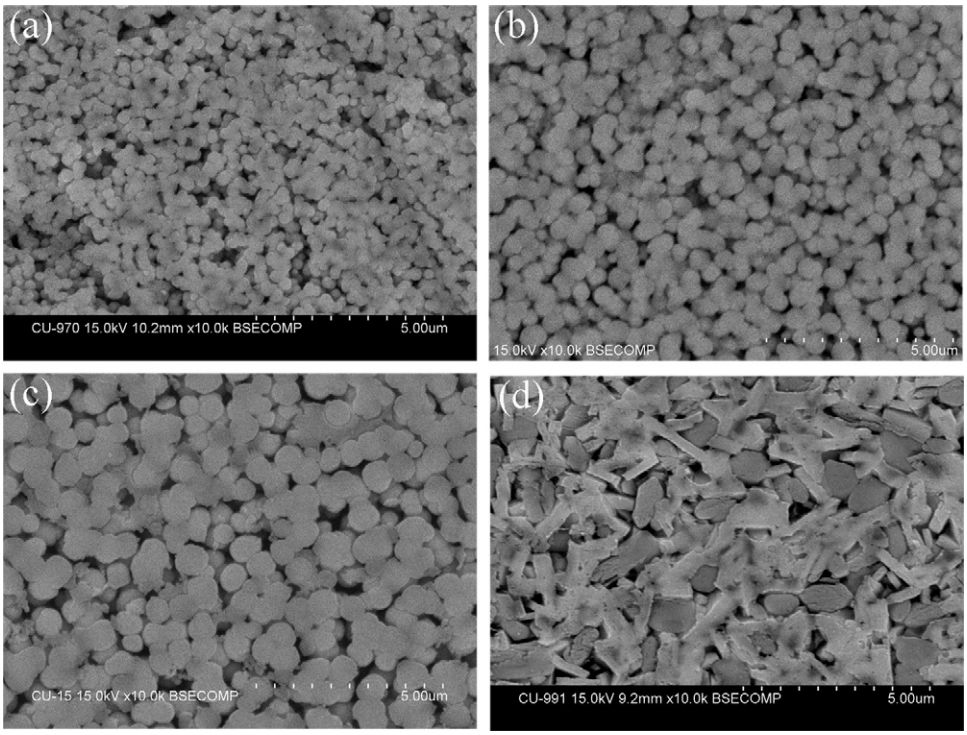

Fig. 4. SEM photograph of polished and etched surface of Ba03 nucleated at 700 °C for 2 h and crystallized at 800 °C (a), 900 °C (b), 1000 °C (c) and 1150 °C (d) for 5 h.

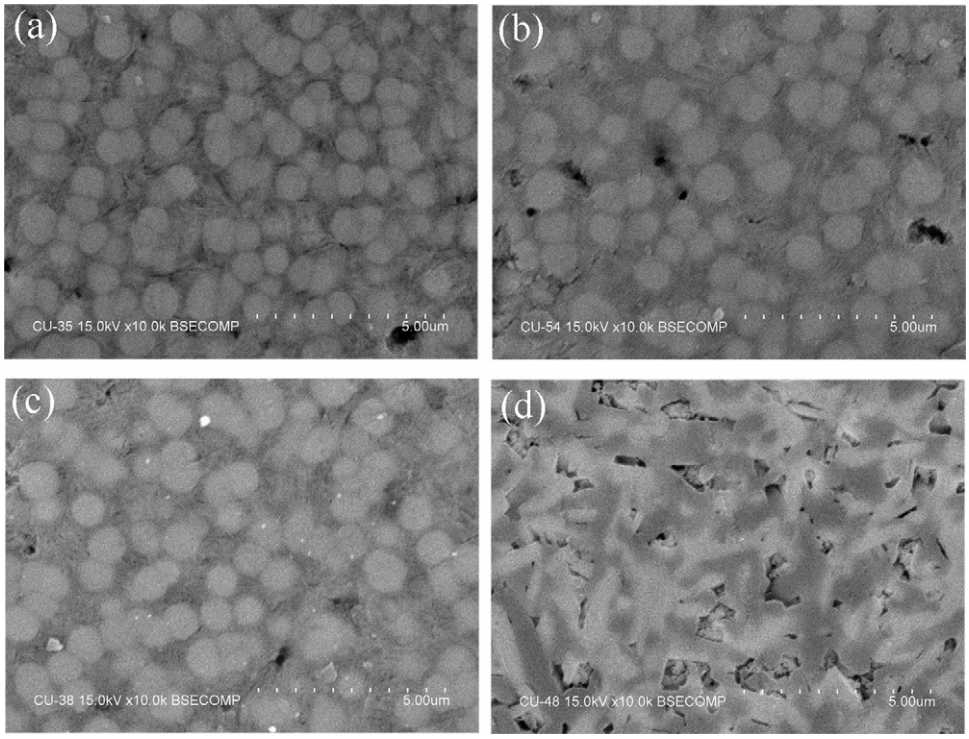

Fig. 5. SEM photograph of polished and etched surface of Ba05 nucleated at 720 °C for 2 h and crystallized at 800 °C (a), 900 °C (b), 1000 °C (c) and 1150 °C (e) for 5 h.

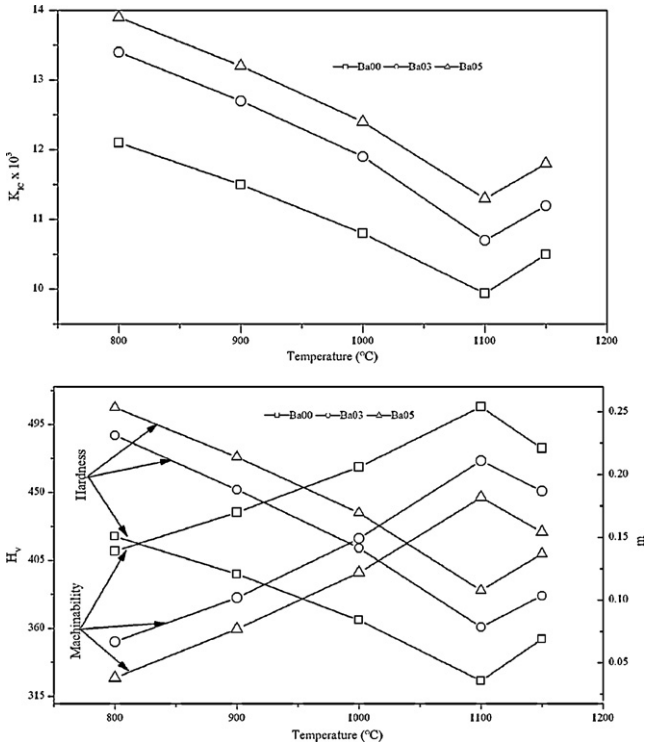

Fig. 6. Vickers hardness (H_v), machinability (m) and fracture toughness (K_{IC}) against different heat treatment temperatures for Ba00, Ba03 and Ba05 samples.

decreasing cutting speed with small cutting force [25,26]. Hardness, machinability and fracture toughness were found to be highly dependent on the formation of interconnected 'house of cards' microstructures.

4. Conclusions

(a) Partial substitution of potassium by barium can lead to the formation of K-fluorophlogopite and Ba-fluorophlogopite crystal phases simultaneously, and forms interconnected ''house of cards'' microstructure.
(b) Fully substituted potassium with barium has the highest hardness, fracture toughness and lowest machinability.
(c) Hardness, machinability and fracture toughness were found to be highly dependant on the formation of an interconnected ''house of cards'' microstructure and aspect ratio of the formed crystals.
(d) Machinability and strength can be customized by judicious substitution of potassium by barium and also by the time of crystallization.

Acknowledgements

Financial support from University Grant Commission (UGC), under Major Research Project is gratefully acknowledged. SEM and XRD facility have been provided by technical education quality improvement programme. One of the authors, Amit Mallik thanks University Grant Commission (UGC), New Delhi, India, for providing junior research fellowship (RGNF).

References

[1] D.S. Baik, K.S. No, J.S. Chun, Y.J. Yoon, H.Y. Cho, A comparative evaluation method of machinability for mica-based glass–ceramics, J. Mater. Sci. 30 (1995) 1801–1806.

[2] G.H. Beall, in: L.L. Hench, S.W. Frieman (Eds.), Advances Nucleation and Crystallization in Glasses, American Ceramic Society, Westerville, 1971, p. 251.
[3] S.N. Hoda, G.H. Beall, in: J.H. Simmons, D.R. Uhlmann (Eds.), Alkaline earth mica glass ceramics, advances in ceramics: nucleation and crystallization in glasses, J. Am. Ceram. Soc. 2 (1982) 287–300.
[4] T. Uno, T. Kasuga, K. Nakjima, High-strength mica containing glass–ceramics, J. Am. Ceram. Soc. 74 (1991) 3139–3141.
[5] J. Henry, R.G. Hill, Influence of alumina content on the nucleation crystallization and microstructure of barium fluorphlogopite glass–ceramics based on $8SiO_2YAl_2O_34MgO_2MgF_2BaO$. Part I. Nucleation and crystallization behavior, J. Mater. Sci. 39 (2004) 2499–2507.
[6] J. Henry, R.G. Hill, Influence of alumina content on the nucleation crystallization and microstructure of barium fluorphlogopite glass–ceramics based on $8SiO_2YAl_2O_34MgO_2MgF_2BaO$. Part II. Microstructure, microhardness and machinability, J. Mater. Sci. 39 (2004) 2509–2515.
[7] P.K. Maiti, A. Mallik, A. Basumajumdar, P. Kundu, Influence of fluorine content on the crystallization and microstructure of barium fluorphlogopite glass–ceramics, Ceram. Int. 36 (2010) 115–120.
[8] K. Greene, M.J. Pomeroy, S. Hampshire, R. Hill, Effect of composition on the properties of glasses in the K_2O–BaO–MgO–SiO_2–B_2O_3–MgF_2 system, J. Non-Cryst. Solids 325 (2003) 193–205.
[9] G.H. Beall, Mica glass–ceramics, US Patent No. 3,689,923, 1972.
[10] B.R. Lawn, D.B. Marshall, Hardness, toughness, and brittleness: an indentation analysis, J. Am. Ceram. Soc. 62 (1979) 347–350.
[11] I.W. Donald, R.A. McCurrie, microstructure and indentation hardness of an MgO–LiO_2–Al_2O_3–SiO_2–TiO_2 glass–ceramics, J. Am. Ceram. Soc. 55 (1972) 289–291.
[12] J. Henry, R.G. Hill, The influence of lithia content on the properties of fluorophlogopite glass–ceramics. 1. Nucleation and crystallization behavior, J. Non-cryst. Solids 319 (2003) 1–12.
[13] N.S. Bagdassarov, Viscoelastic behavior of mica-based glass-ceramic aggregate, Phys. Chem. Miner. 26 (1999) 513–520.
[14] Y. Hu, H.T. Tsai, The effect of BaO on the crystallization behaviour of a cordierite-type glass, Mater. Chem. Phys. 52 (1998) 184–188.
[15] K. Matusita, S. Saka, Kinetic study of crystallization of glass by differential thermal analysis—criterion on application of Kissinger plot, J. Non-Cryst. Solids 39 (1980) 741–746.
[16] J.A. Augis, J.E. Bennett, Calculation of the Avrami parameters for heterogeneous solid state reactions using a modification of the Kissinger method, J. Therm. Anal. 13 (1978) 283–292.
[17] K. Cheng, Evaluation of crystallization kinetics of glasses by non-isothermal analysis, J. Mater. Sci. 36 (2001) 1043–1048.
[18] Y.J. Park, J. Heo, Nucleation and crystallization kinetics of glass derived from incinerator fly ash waste, Ceram. Int. 28 (6) (2002) 669–673.
[19] L.A. Perez-Maqueda, J.M. Criado, J. Malek, Combined kinetic analysis for crystallization kinetics of non-crystalline solids, J. Non-Cryst. Solids 320 (1–3) (2003) 84–91.
[20] C.K. Chyung, G.H. Beall, D.G. Grossman, Fluorphlogopite mica glass–ceramics, in: Proc. International Glass Congress, No. 14, Kyoto, Japan, Ceramic Society of Japan, Tokyo, Japan, 1974, pp. 33–40.
[21] K.G. Cheng, J.L. Wan, K.M. Liang, Hot-pressed mica glass–ceramics with high strength and toughness, J. Am. Ceram. Soc. 82 (1999) 1633–1634.
[22] Z. Strnad, −110 in glass-ceramic materials: liquid phase separation, nucleation and crystallization in glasses, Glass Science and Technology, vol. 8, Elsevier, Amsterdam, New York, 1986, p. 109.
[23] T. Uno, T. Kasuga, S. Nakayama, Microstructure of mica-based nanocomposite glass–ceramics, J. Am. Ceram. Soc. 76 (1993) 539–543.
[24] D.G. Grossman, Machinable glass–ceramics based on tetrasilisic mica, J. Am. Ceram. Soc. 55 (1972) 446–449.
[25] D.S. Baik, K.S. No, J.S. Chun, H.Y. Cho, Effect of the aspect ratio of mica crystals and crystallinity on the microhardness and machinability of mica glass–ceramics, J. Mater. Process. Technol. 67 (1997) 50–54.
[26] D.S. Baik, K.S. No, J.S.S. Chun, Y.J. Yoon, Mechanical properties of mica glass–ceramics, J. Am. Ceram. Soc. 78 (1995) 1217–1222.